Article

An Non-Uniform Interference-Fit Size Investigation of CFRP/Al-Alloy by Riveting Mold Design

Xingxing Wang[1,2]*, Zhenchao Qi[2], Mu Lu[3] and Haicheng Pan[1]

[1]College of Mechanical and Electrical Engineering, Suqian University, Suqian 223800, China
[2]College of Mechanical and Electrical Engineering, Nanjing University of Aeronautics and Astronautics, Nanjing 210016, China
[3]Jiangsu Geri Technology Co., LTD
Correspondence: wangxx@squ.edu.cn; Tel: 18805199328

Abstract: The interference-fit size has a significant effect on CFRP/Al-alloy laminates riveted lap joints, the requirements for the interference-fit size are different because of the strengthening of heterogeneous materials. However, in the process of the riveted CFRP/Al-alloy, the heterogeneous laminates lead to poor structural strength because of the different requirements of interference-fit size. Therefore, the different assembly types of riveting mold are designed to acquire a novel interference-fit size, and the tensile test is adopted to evaluate the tensile property. In addition, the fracture failure of CFRP/Al-alloy laminates riveted lap joint is observed by the ultra-depth of field microscope. Finally, the best assembly type is the trapezoid riveting mold combined with an arc riveting die, and the sidewall intersection angle of the trapezoid riveting mold is 66° which could achieve a suitable interference-fit size and a better mechanical performance.

Keywords: CFRP/Al-alloy; assembly type of riveting mold; interference-fit size; mechanical performance

1. Introduction

Due to its high specific strength and modulus of characteristics of Carbon fiber reinforced plastics (CFRP), which has been wildly applied in the transportation industry [1]. At present, the CFRP/Al-alloy riveted lap joints are used the 2%~3% of interference-fit size[2], which validly improves the Al-alloy sheet connection performance[3]. Mirzajanzadeh et al. [4] found that large interference-fit size can increase the fatigue life of Al alloy sheets in fretting fatigue crack properties. Abazadeh et al. [5] investigated the Al-alloy sheets bolted joints, the results proved that a larger interference-fit size is beneficial to improving Al-alloy sheets bolted joint's performance.

However, it's a double-edged sword of larger inference-fit size for CFRP/Al-alloy riveted lap joint, because the interference-fit size of CFRP sheet riveted lap joint is adopted less than 1.6% [6-7]. Large interference-fit size can induce extrusion, instability, and delamination of CFRP's hole surface, particularly the entrance of connection surface is over 2% [8-9]. Khashaba et al. [10] proposed a predicated 3D progressive damage model between clearance-fit sizes and static strength of CFRP joint. Chen et al. [11] studied the effects of zero-fit, clearance-fit, and interference-fit size on the CFRP joints' mechanical performance, the results showed that the zero-fit or clearance-fit of joints had a better shear performance than the interference-fit. Zou et al. [12] developed a FEM model to predicate the effect of interference-fit size on delamination defect, the result showed that the increase of interference-fit size worsened the delamination of CFRP.

The abovementioned studies are homogeneous laminates, hence the interference-fit size could be adjusted to suit them, simply. Nevertheless, during the heterogeneous laminates of CFRP/Al-alloy riveting, its interference-fit size is different from the homogeneous laminates'[13]. It still adopted the traditional riveting process, which easily leads to an excessive interference-fit size for CFRP or an undersize interference-fit size for Al-alloy.

 doi:10.20944/preprints202302.0455.v1

Therefore, researchers have studied the way to improve the mechanical performance of CFRP/Al-alloy laminates riveting lap joints. Cui et al. [13] investigated the effect of trapezoid riveting mold on interference-fit size, the result proved that mold angle had a significant effect on interference-fit size. Jiang et al. [15] studied the CFRP/Al-alloy laminates by electromagnetic riveting with different riveting molds, the result showed that the 80° trapezoid riveting mold can not only improve the interference-fit size but also promote the fatigue performance. Ma et al. [16] developed an effective way to avoid the joints cracking by riveting mold structure optimization. Although scholars have adopted the riveting mold design to investigate the interference-fit size and achieve a better mechanical performance, the interference-fit sizes of CFRP sheet and Al-alloy sheet are still the same without considering the material difference. How to make the interference-fit size of CFRP/Al-alloy more suitable still need further research. Therefore, the optimal design of die not only can improve material flow and mechanical properties, but also reduce the forming load [17-19]. Besides, for the purpose of shorting the cycle and saving cost, lots of scholars adopted the FEM and experiment method to carry out research [20]-23].

It is acknowledged that the interference fit of CFRP riveted lap joints lead to instability of fiber and weaken the performance with it increase [24-25]. Therefore, in this paper, not only the design parameters of riveting mold are researched, but also the assembly types of riveting mold. Primarily, the design parameters of the riveting mold are analyzed by FEM, and the significant effect parameter is confirmed. Furthermore, the riveting experiments are carried out, and the interference-fit size is measured. Finally, the tensile test is performed to ensure the structure of the riveting mold, and the fatigue failure types and microstructure performance are observed.

2. Materials and Methods

2.1. Sample preparation

The T700 CFRP and 2024 Al-alloy were selected for adapting piece, the material of the rivet is Ti-45Nb. T700 CFRP was using a unidirectional carbon fiber/epoxy with a thickness of 0.15mm per ply (provided by GW COMPOS Company Ltd., China). The fabricated T700 CFRP laminate processes a thickness of 2.3 mm with 16 piles, the ply orientation of T700 CFRP is [0°/90°/45°/-45°/-45°/45°/90°0°]2s, and the weight fraction of carbon fiber is about 60%. Material properties of the fabricated CFRP laminates are presented in **Error! Reference source not found.**. Moreover, the Fabricated Ti-45Nb rivets (provided by CAG Company Ltd., China) were annealed by heating in a vacuum (less than 0.1um mercury) to a temperature within the range of 1450 °F to 1600 °F, holding at heat for sufficient time to produce a recrystallized structure that will meet the requirements of 3.5. Material properties of the Ti-45Nb rivets are presented in **Error! Reference source not found.**. In addition, the diameter of the Ti-45Nb rivet is 4mm, and the prefabricated hole diameters of CFRP laminates were drilled by dagger drill with a diameter of 4.1mm, and the aperture of the sample was measured using a plug gauge. The sizes of CFRP riveted specimens according to the ASTM D5661 are shown in Fig. 3, and W/D≥6, E/D≥3.

Table 1. Mechanical properties of the sample.

CFRP laminates		Ti-45Nb rivets	
Property	Value	Property	Value
Resin content(%)	40	Density [g/cm3]	5.7
Tensile strength(Mpa)	2300	Poisson ratio	0.34
Tensile modulus(Gpa)	115	Tensile modulus [GPa]	62
Flexural strength (Mpa)	1250	Yield strength [MPa]	425
Compressive strength (Mpa)	1050	Tensile strength [MPa]	570
Interlaminar shear strength (Mpa)	55		

Preprints (www.preprints.org) | NOT PEER-REVIEWED | Posted: 27 February 2023 doi:10.20944/preprints202302.0455.v1

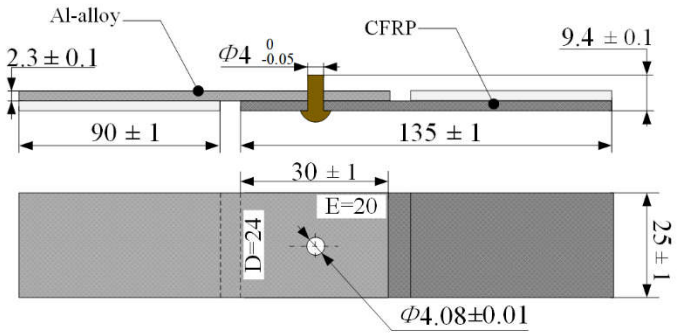

Figure 1. Dimensions of the CFRP laminates riveted lap joint (dimension in mm).

2.2. Experimental results handling method

It acknowledged that the large interference-fit size induced the CFRP damage, hence, the ideal interference-fit size for CFRP/Al-alloy laminates is as shown in **Error! Reference source not found.**. The interference-fit size of CFRP should be less than Al-alloy's. Therefore, to acquire the ideal fit of CFRP/Al-alloy riveted lap joint, the mold of the rivet mechanical head (bottom mold) is used as an arc riveting mold (ARM) to prevent the deformation of rivet mechanical head, so fit at the entrance of CFRP connection surface is clearance. The mold of the rivet bar (top mold) is used flat riveting mold (FRM) or trapezoid riveting mold (TRM), hence, the assembly types of riveting mold are shown in **Error! Reference source not found.**. In the riveting process, the interface slip of the die and rivet would produce the radial constraint force which can promote material filling the hole. Considering the larger interference-fit size of Al-alloy, assembly type 2 of riveting mold is adopted to research the variation of interference-fit size.

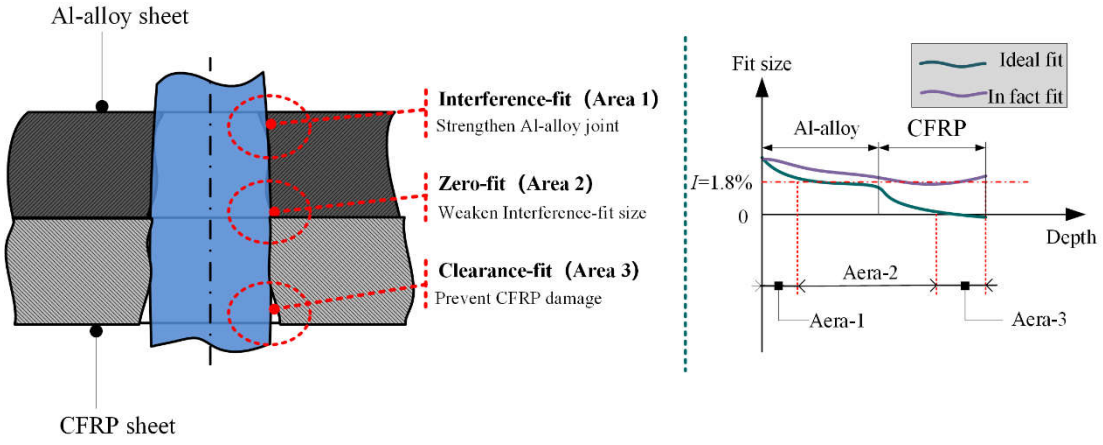

Figure 2. Two interference fit curves of composite/Al alloy sheets.

Preprints (www.preprints.org) | NOT PEER-REVIEWED | Posted: 27 February 2023 doi:10.20944/preprints202302.0455.v1

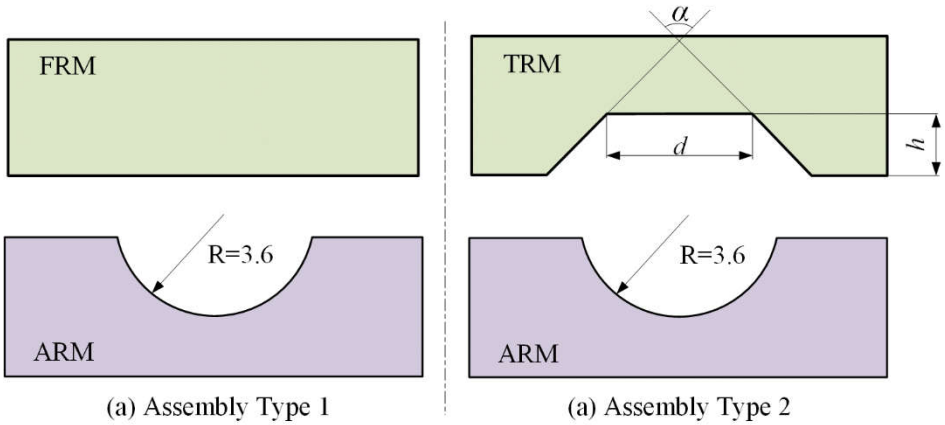

Figure 3. Different assembly types of riveting mold.

After the riveting, the deformed rivet specimens are cut with diamond blades. The interference-fit size of the deformed rivet bar is measured by a Vernier caliper with an accuracy of 0.01mm. subsequently, the DBSL-10t tensile test machine was used to test the mechanical properties of riveted specimens under pull-out loading based on the ASTM-5961 standard. Finally, microstructures of fracture morphology were observed by the RH-2000 super-depth microscopy system.

3. Results

3.1. The combination type of rivet dies

Combination type design of rivet die is an effective way to achieve the non-uniform interference fit of CFRP/Al alloy sheets. As shown in **Error! Reference source not found.**a, the effect of rivet die combination types on interference sizes tendency was preliminarily analyzed by FEM, which included four kinds of types, i.e. flat rivet die (FRD) to flat rivet die, flat rivet die to arc rivet die (ARD), trapezoid rivet die (TRD) to flat rivet die, trapezoid rivet die to arc flat die. It could be seen that the type of TRD-ARD or FRD-ARD could obtain the non-uniform interference fit. Meanwhile, to ensure the non-uniform interference sizes are reasonable, the TRD-ARD type need be optimized. **Error! Reference source not found.**b showed the structure of TRD-ARD type. The trapezoid rivet die parameters include the sidewall intersection angle (α), sidewall height (h) and upper diameter of sidewall (d). According to the constant volume principle, the structure parameters of TRD had significant influences on the material filling into the pre-drilled hole. The arc rivet die matched with the rivet manufactured head, the radial is 3.6mm, depth is 2.0mm.

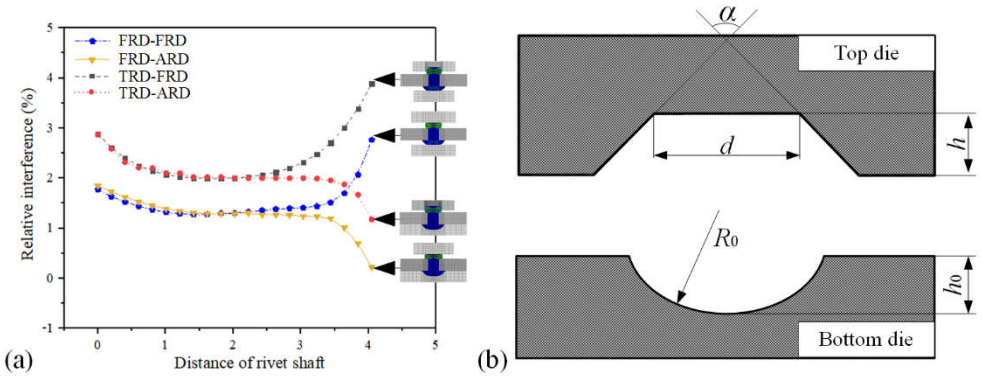

Figure 4. a) Interference fit tendency for different combination of rivet dies; (b) The combination type rivet dies for non-uniform interference fit.

Preprints (www.preprints.org) | NOT PEER-REVIEWED | Posted: 27 February 2023 doi:10.20944/preprints202302.0455.v1

3.2. Rivet radial force constrain modelling

In riveting process, the interface slip of die and rivet would produce the radial constraint force which can promote material filling the hole. Considering the isotropic material and axisymmetric structure of rivet, the radial force is as homogeneous distribution. The diagram of central section radial force was presented in **Error! Reference source not found.**. Rivet shaft subjects to the axial force (F_z) and radial force (F_r), the F_r is f_u in flat rivet die which can improve the interference size. The F_z is a constant, hence adopting concave rivet die structure to increase F_r is as an effective way.

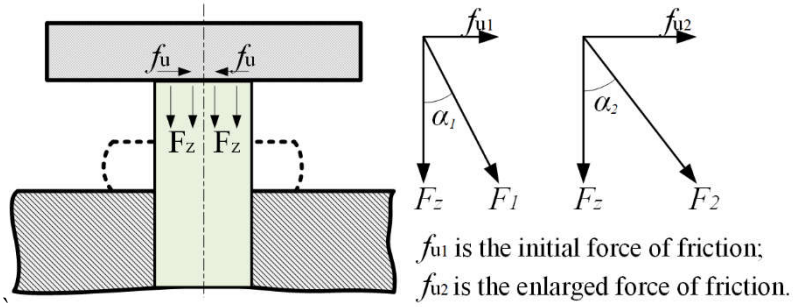

Figure 5. A diagram of central section radial force.

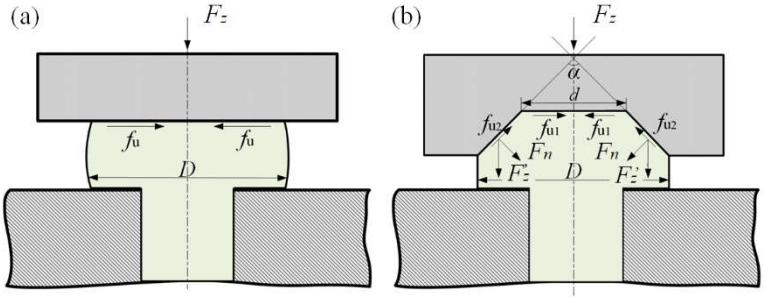

Figure 6. The comparison analysis of radial force. (a) Flat rivet die. (b) Special rivet die.

In **Error! Reference source not found.**, the comparison of radial constrain force between FRD and TRD will be analyzed as follows. As shown in Fig.7a, the radial constrain force of flat rivet die (F_{frd}) is simple friction (f_u), as following Eq. (1):

$$F_{frd} = f_\mu = \frac{1}{2} F_z \cdot \mu \tag{1}$$

As shown in Fig.7b, the radial constrain force of trapezoid rivet die (F_{trd}) includes horizontal friction (f_{u1}), horizontal component of f_{u2} and F_n, as following Eq. (2):

$$\begin{cases} F_{srd} = F_r = f_{\mu 1} + f_{\mu 2} \cdot \sin\dfrac{\alpha}{2} + F_n \cdot \cos\dfrac{\alpha}{2} \\ f_{\mu 1} = \dfrac{1}{2} F_z \cdot \dfrac{d}{D} \cdot \mu \\ f_{\mu 2} = F_z' \cdot \cos\dfrac{\alpha}{2} + F_n \cdot \mu \\ F_n = F_z' \cdot \sin\dfrac{\alpha}{2} \\ F_z' = \dfrac{1}{2} F_n \cdot \dfrac{D-d}{D} \end{cases} \tag{2}$$

Therefore, when the F_{trd} is larger than F_{frd}, combined Eq. (1) with Eq. (2) to obtain the function of α and μ, as following Eq. (3):

$$2\tan\frac{\alpha}{2} > \mu \tag{3}$$

Preprints (www.preprints.org) | NOT PEER-REVIEWED | Posted: 27 February 2023 doi:10.20944/preprints202302.0455.v1

where 0 <α<180°, and μ≈0.2 (Normally, the friction coefficient of upsetting is 0.2.), then substitute them into Eq. (3), we obtained 12°<α<180°.

4. Discussion

According to the size of the rivet mechanical head, the radius of ARM is 3.6 mm, and they remain the same. However, the parameters of TRM include the sidewall intersection angle (α), sidewall height (h), and upper diameter of sidewall (d), the level of the parameters is shown in **Error! Reference source not found.**, and total schemes are 16 ($L3^4$). The FEM model is established by Deform-3D, as shown in **Error! Reference source not found.**a, and the variation of interference-fit sizes is shown in **Error! Reference source not found.**b ~ **Error! Reference source not found.**f. The maximum interference-fit size (I_{max}) is counted in **Error! Reference source not found.**.

The deviations of the parameters are listed in **Error! Reference source not found.**, it could be seen that the significance of parameters on interference-fit size is $\alpha > d > h$, which is consistent with the before research. In **Error! Reference source not found.**, the collecting points of the rivet bar are shown in the red circle, comparing FRM with the TRM, the TRM improves the interference-fit size, significantly, and the interference-fit size in the entrance of the CFRP connection surface is reduced by ARM. Then the decision tree model is developed and adopted to repetitively train the data of **Error! Reference source not found.**, the trained weight for variables are displayed in **Error! Reference source not found.**. It could be seen that The average weight value of α, d, and h for interference-fit size are 0.65, 0.24, 0.11 respectively. To sum up, the weight values of α for load and interference are the most significant.

According to **Error! Reference source not found.**c ~ **Error! Reference source not found.**f, the reasonable schemes of interference-fit size are scheme 2, scheme 6, scheme 9, and scheme 15. Considering the significance of parameters, schemes 6, 9, 15 are adopted to implement the experimental verification. Finally,

Table 2. Parameters level of TRM structure.

Variable	Level 1	Level 2	Level 3	Level 4
H/mm	1.6	1.8	2.0	2.2
d/mm	4.2	4.4	4.6	4.8
α	22°	44°	66°	88°

Table 3. The schemes and results of the research design.

Scheme	h/mm	d/mm	α/°	I_{max} /%
1	1.6	4.2	22	3.70
2	1.6	4.4	44	2.49
3	1.6	4.6	66	2.01
4	1.6	4.8	88	2.45
5	1.8	4.2	44	4.37
6	1.8	4.4	22	3.41
7	1.8	4.6	88	2.34
8	1.8	4.8	66	2.30
9	2.0	4.2	66	2.92
10	2.0	4.4	88	2.48
11	2.0	4.6	22	3.65
12	2.0	4.8	44	2.81
13	2.2	4.2	88	2.72
14	2.2	4.4	66	2.70
15	2.2	4.6	44	3.15
16	2.2	4.8	22	3.58

Preprints (www.preprints.org) | NOT PEER-REVIEWED | Posted: 27 February 2023 doi:10.20944/preprints202302.0455.v1

Table 4. The I_{max} average of each variable.

Level	h/mm	d/mm	α
1	2.662	3.428	3.585
2	3.105	2.770	3.205
3	2.965	2.788	2.482
4	3.038	2.785	2.498
Deviation max-min	0.443	0.657	1103

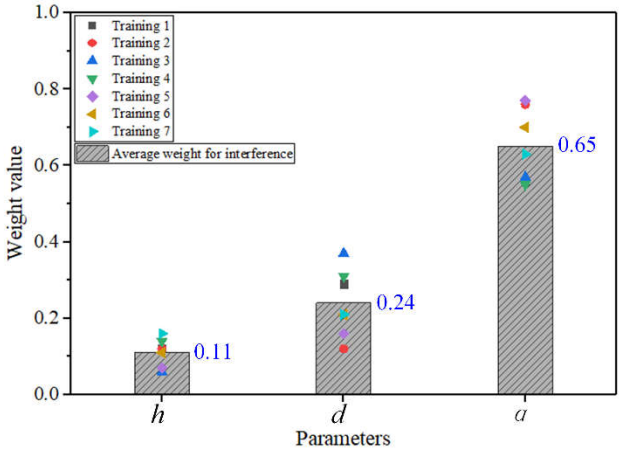

Figure 7. The weight for interference-fit size by decision-making tree.

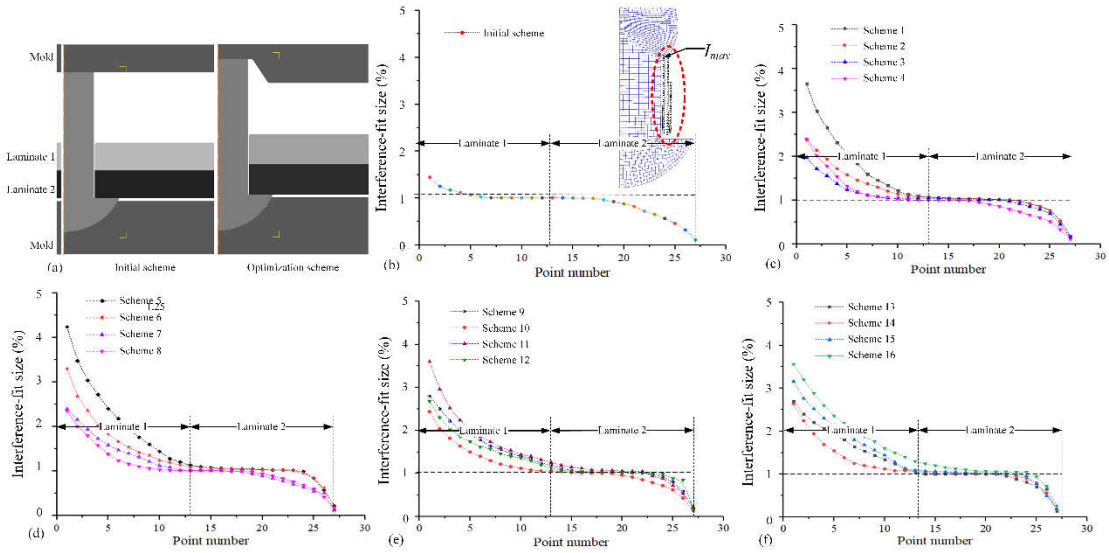

Figure 8. The variation process of the interference-fit size.

4.1. Non-uniform interference-fit size

According to the interference sizes effect analysis, the TRM based on the parameters of scheme 6, scheme 9, and scheme 15 are manufactured, and the manufactured FRM is as the contrast experiment, as shown in **Error! Reference source not found.**. The force and speed of riveting process are 14.5KN and 10mm/s, respectively. After riveting, the inter-

Preprints (www.preprints.org) | NOT PEER-REVIEWED | Posted: 27 February 2023 doi:10.20944/preprints202302.0455.v1

ference-fit size of each specimen is measured with five positions, as shown in **Error! Reference source not found.**. The measured interference-fit size is listed in **Error! Reference source not found.** with three times of repetition, then taking an average of interference-fit size (I_A).

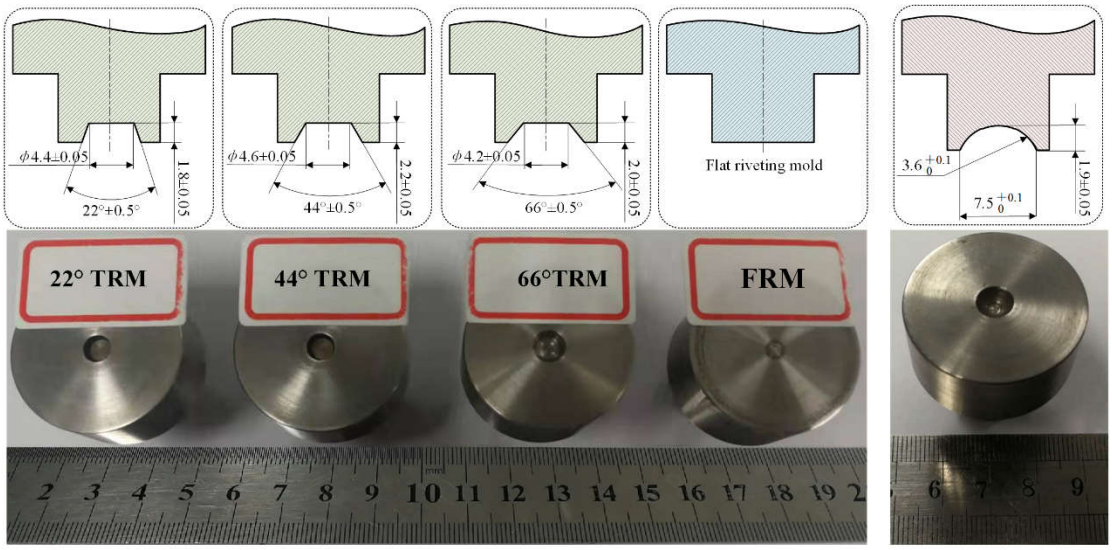

Figure 9. Dimensions and products of different riveting molds.

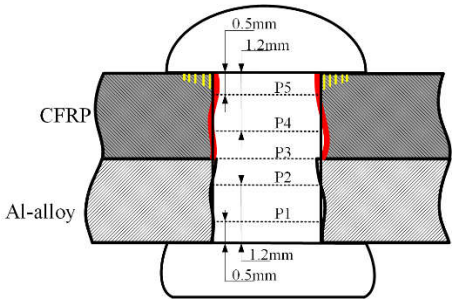

Figure 10. Measurement positions of Interference-fit size.

Table 5. the measured results of relative interference for different rivet dies.

Type	Position	Repeat 1(mm)	Repeat 2(mm)	Repeat 3(mm)	Average value (mm)	I_A (%)
FRM	1	4.16	4.17	4.16	4.163	2.03
	2	4.13	4.13	4.13	4.130	0.98
	3	4.12	4.10	4.12	4.130	0.98
	4	4.11	4.12	4.11	4.113	0.809
	5	4.10	4.12	4.12	4.113	0.809
22° TRM	1	4.19	4.20	4.18	4.190	2.70
	2	4.17	4.16	4.16	4.163	2.03
	3	4.14	4.15	4.15	4.147	1.64
	4	4.13	4.12	4.13	4.127	1.15
	5	4.10	4.10	4.10	4.100	0.74
44° TRM	1	4.21	4.20	4.21	4.207	3.11
	2	4.18	4.17	4.19	4.180	2.45
	3	4.15	4.15	4.15	4.150	1.72
	4	4.14	4.13	4.14	4.137	1.40
	5	4.12	4.13	4.13	4.127	1.15
66° TRM	1	4.19	4.18	4.19	4.187	2.63
	2	4.18	4.18	4.17	4.177	2.38
	3	4.14	4.14	4.13	4.137	1.40

Preprints (www.preprints.org) | NOT PEER-REVIEWED | Posted: 27 February 2023 doi:10.20944/preprints202302.0455.v1

4	4.14	4.13	4.14	4.137	1.40
5	4.13	4.11	4.13	4.123	1.05

To intuitively analyze the data in **Error! Reference source not found.**, the date histograms of different riveting molds are implemented in **Error! Reference source not found.**. **Error! Reference source not found.**a displayed the interference-fit size of FRM-ARM, it could be seen that the max interference-fit size is lower than 2%, and the CFRP sheet fit well. However, the interference-fit size of the Al-alloy sheet was not satisfied with the requirement. In **Error! Reference source not found.**b and **Error! Reference source not found.**c, the results show that the variation tendency of interference-fit size by 22° TAM-ARM and 44° TAM-ARM have a good consistency. However, both of them were non-uniform interference-fit sizes in independent Al-ally and CFRP. In **Error! Reference source not found.**e, the variation tendency of interference-fit size by 66° TAM-ARM presents a good consistency with the ideal interference-fit size. In addition, the interference-fit size is relatively uniform for each laminate. Therefore, based on the variation tendency of interference-fit size, the 66° TAM-ARM is a better assembly type than others.

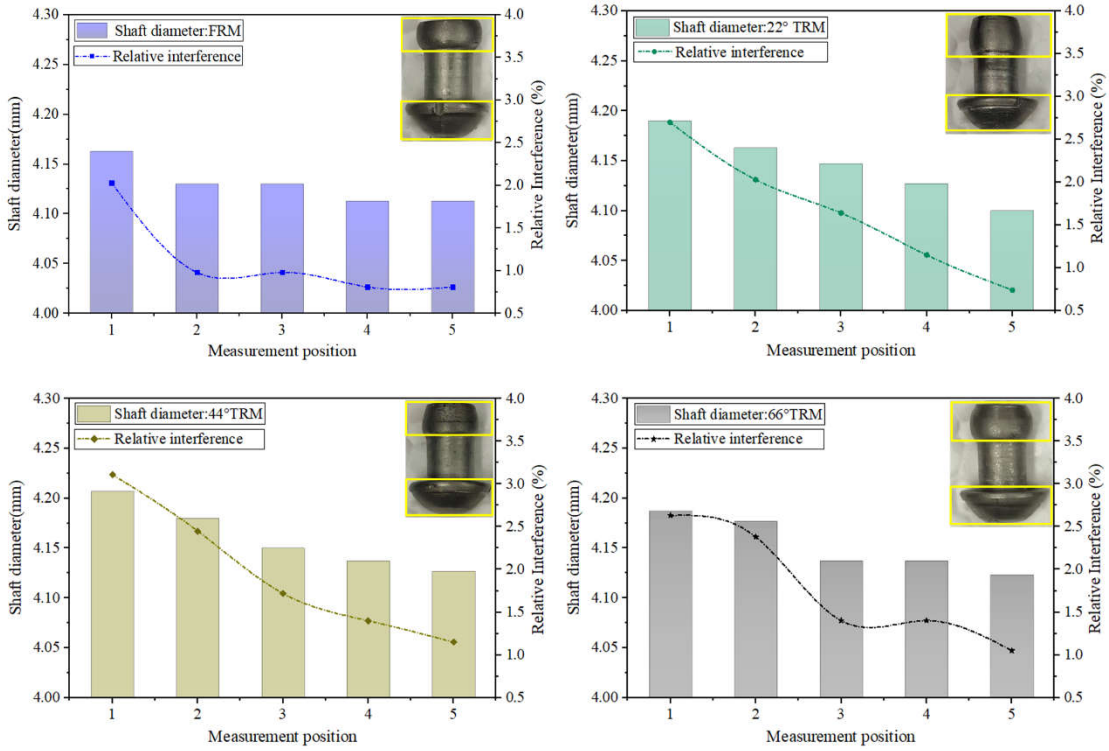

Figure 11. Diameter and interference-fit size analysis with different riveting molds.

4.2. Strength and fracture modes

To research the effect of interference-fit size with different riveting molds on the strength of CFRP/Al-alloy riveted lap joints, the tensile test is carried out at a speed of 5mm/min. The tensile load-displacement curves of 22°-TRM, 44°-TRM, and 66°-TRM are displayed in **Error! Reference source not found.**. It could be seen that the tensile load rises rapidly with the increase of displacement in the elastic deformation stage. However, the load-displacement curves in the failure stage presented distinct differences, especially the riveted specimen by 66°-TRM. For the riveted specimens by 22°-TRM and 44°TRM, the pulled-off failure displacement is longer than 66°-TRM. In addition, the max tensile load (5734N) of the specimen is riveted by 66°-TRM, which is a litter higher than 44°-TRM's (5709N), both of them are larger than the max tensile load (5118N) by 22°-TRM.

Preprints (www.preprints.org) | NOT PEER-REVIEWED | Posted: 27 February 2023 doi:10.20944/preprints202302.0455.v1

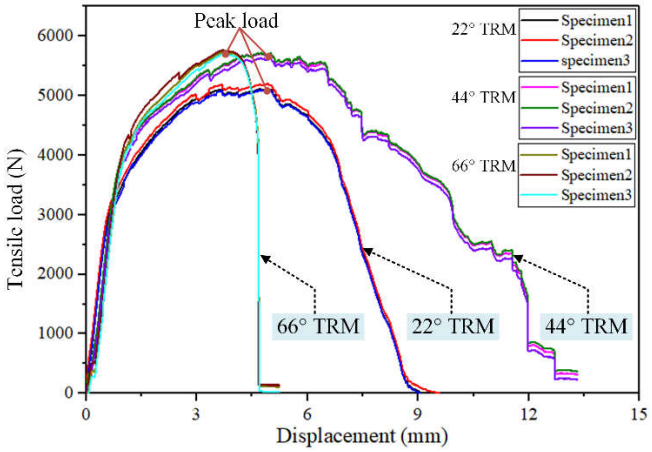

Figure 12. The tensile load-displacement curves with different angles of TRM.

Furtherly, the failure types of specimens by different TRM are shown in **Error! Reference source not found.**. It could be seen that the failure type of specimens by 22°-TRM and 44°-TRM is rivet pull-out, but the failure type of specimens by 66°-TRM is rivet shear fracture. This induces a longer failure displacement of tensile test of specimens by 22°-TRM and 44°-TRM, and the failure displacement of specimens by 66°-TRM is short. Combined with **Error! Reference source not found.** to reveal the difference in failure type, for specimens 22°-TRM and 44°-TRM, the interference-fit size in the entrance of Al-alloy by 44°-TRM's specimen is larger than 22°-TRM's under the same riveting force. Hence, the strength of the Al-alloy riveted lap joint by 44°-TRM is larger than 22°-TRM's, and the strength of the Al-alloy riveted lap joint is larger than the CFRP riveted lap joint by 44°-TRM, and the strength of Al-alloy and CFRP by 22°-TRM is on the contrary. In addition, the interference-fit size is non-uniform for each sheet. Both reasons induce the rivet pull-out from the sheet. However, the relative uniform interference-fit size by 66°-TRM well reinforces the fit strength of Al-alloy and CFRP, and the interference-fit size is satisfied with the requirement, both reasons induce the rivet shear fracture.

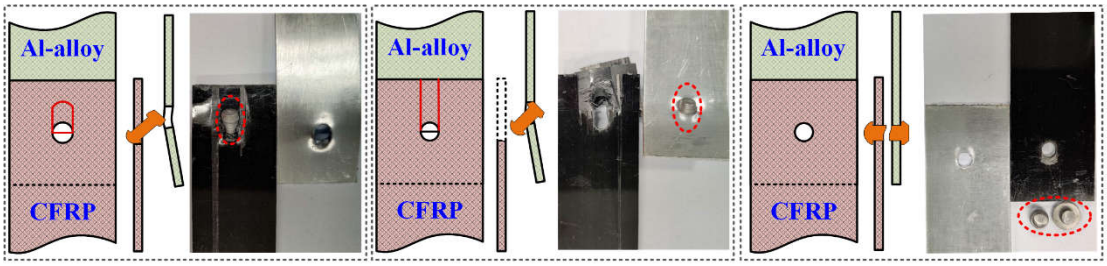

(a) Rivet pull-out from Al-ally **FRM-ARM/ 22°TRM-ARM** (b) Rivet pull-out from CFRP **44°TRM-ARM** (c) Rivet shear fracture **66°TRM-ARM**

Figure 13. The typical fracture modes for different riveting molds.

4.3. Fracture microstructure

The failure morphology is observed by microscope. In **Error! Reference source not found.**, the microstructure of the specimens' pull-out hole by 22°-TRM is observed. The hole of Al-alloy is stretched, and the hole shows relatively smooth and does not appear to crack, which stays in the plastic deformation extension stage. The observed CFRP's positions are shown in **Error! Reference source not found.**a, corresponding to **Error! Reference source not found.**d to **Error! Reference source not found.**g, respectively. It could be seen that the carbon fiber of the P_1 position does not occur delamination or extrusion damage. P_2 position shows that the 45°/-45°/90° carbon fibers are suffered from extrusion. Carbon fibers of the P_3 position are subjected to tension and extrusion, which induced a part

Preprints (www.preprints.org) | NOT PEER-REVIEWED | Posted: 27 February 2023 doi:10.20944/preprints202302.0455.v1

of the carbon fibers to snap. In the P_4 position, the CFRP hole occurs severe extrusion, and delamination and carbon fiber breakage appear.

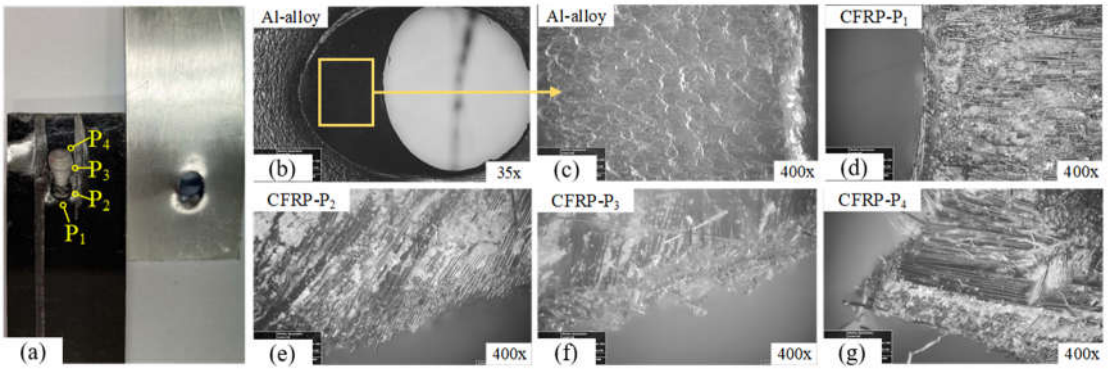

Figure 14. The specimen fracture morphology of 22° TRM.

The failure microtopography of specimens by 44°-TRM is shown in **Error! Reference source not found.**. It could be seen that the CFRP's damage is much more serious than the specimens by 22°-TRM, the observed positions are shown in **Error! Reference source not found.**a. In **Error! Reference source not found.**b, it could be seen that the carbon fibers in P1 are peeled off. As the rivet is pulled out, the carbon fibers were sheared, and severe delamination defect of CFRP is occurred, as shown in **Error! Reference source not found.**c and **Error! Reference source not found.**d. In **Error! Reference source not found.**e, the P_4 position of CFRP sheet occurs severe fracture, where carbon fibers are seriously snapped and crushed.

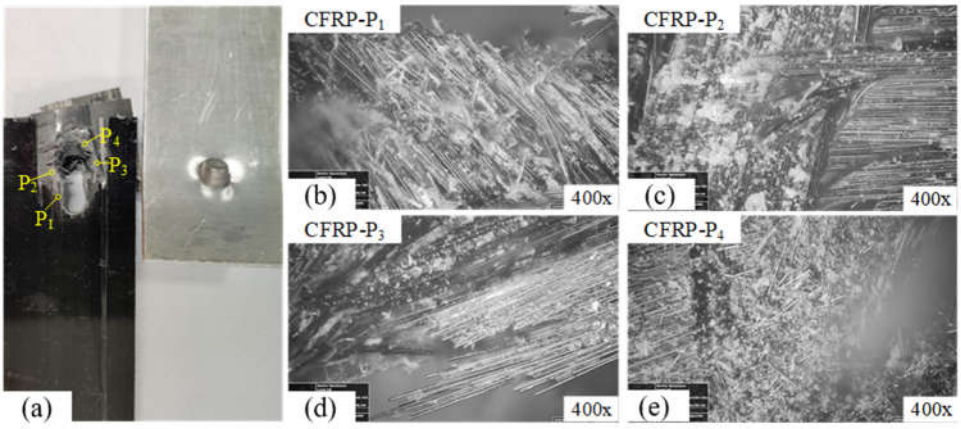

Figure 15. The specimen fracture morphology of 44° TRM.

The failure mode of the specimen by 66°-TRM is shown in **Error! Reference source not found.**. It could be seen that the CFRP and Al-alloy keep well, and the rivet occurs shear fracture. In **Error! Reference source not found.**a, according to the symmetrical fracture surface of the rivet, it is divided into three zones, i.e., shear source (zone 1), ductile fracture (zone 2), and brittle fracture (zone 3). In **Error! Reference source not found.**b, the fracture microstructure in zone 1 is relatively smooth and has a distinct transition area. The transition area displays an elongating shear-long micro-pit, then gradually develops into a ductile fracture area and brittle fracture area, as shown in **Error! Reference source not found.**c. The ductile fracture in zone 2 is a shear-long micro-pit, as shown in **Error! Reference source not found.**c. It indicates that the material has undergone the severe shear deformation under low strain ratio. The brittle fracture morphology in zone 3 is shown in **Error! Reference source not found.**d. It is a typical inter-crystalline delamination fracture, which indicates poor plasticity of the Ti-45Nb rivet.

Preprints (www.preprints.org) | NOT PEER-REVIEWED | Posted: 27 February 2023 doi:10.20944/preprints202302.0455.v1

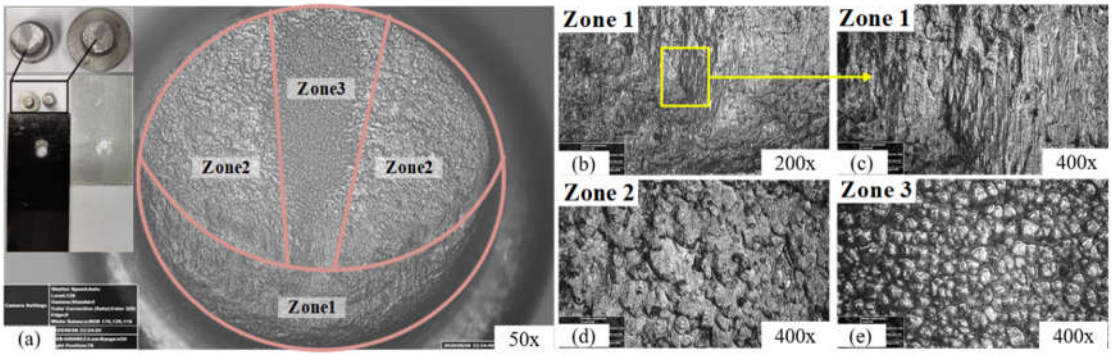

Figure 16. The specimen fracture morphology of 66° TRM.

5. Conclusions

In this research, the assembly types of rivet mold are used to investigate the effect of interference-fit size on the mechanical performance of CFRP/Al-alloy riveted lap joints. The main conclusions are as follows:

The FEM results show: the assembly type of TRM-ARM can acquire a similar ideal fit for CFRP/Al-alloy riveted lap joint; the most significant effect of the design parameter of TRM on interference-fit size is the sidewall intersection angle (α); the average weight value of α for interference-fit size arrives 0.65.

The experiment results show: the TRM-ARM can acquire a larger interference-fit size in an Al-alloy sheet than FAM-ARM; the assembly type of 66° TRM-ARM has a more uniform interference-fit size for each laminate of CFRP and Al-alloy, and the fit surface of hole well reinforce than 22° TRM-ARM and 44° TRM-ARM.

The tensile tests show that the 66° TRM-ARM achieves a better shearing performance than the 22°TRM-ARM and 44°TRM-ARM.

Funding: The authors would like to acknowledge the editors and the anonymous referees for their insightful comments. This work was supported by the Basic Science Research Project of Jiangsu Province (22KJB460008); the Basic Research Plan Natural Science Fund of Suqian Science and Technology Plan Project (K202210); Suqian Science and Technology Plan Guiding Project (Z2021139).

Conflicts of Interest: Declare conflicts of interest or state "The authors declare no conflict of interest." Authors must identify and declare any personal circumstances or interest that may be perceived as inappropriately influencing the representation or interpretation of reported research results. Any role of the funders in the design of the study; in the collection, analyses or interpretation of data; in the writing of the manuscript; or in the decision to publish the results must be declared in this section. If there is no role, please state "The funders had no role in the design of the study; in the collection, analyses, or interpretation of data; in the writing of the manuscript; or in the decision to publish the results".

References

[1]. M. Skorupa, A. Skorupa, T. Machniewicz, Korbel A, Effect of production variables on the fatigue behavior of riveted lap joints, International Journal of Fatigue. 32 (2010) 996–1003.

[2]. X. Zhang, H. Jiang, T. Luo, L. Hu, G.Y. Li, J.J. Cui, Theoretical and experimental investigation on interference fit in electromagnetic riveting, International Journal of Mechanical Sciences. 156 (2019) 261–271.

[3]. C.Y. Lei, Y.B. Bi, J.X. Li, Y.L. Ke, Experiment and numerical simulations of a slug rivet installation process based on different modeling methods, The International Journal of Advanced Manufacturing Technology. 97 (2018) 1481–1496.

[4]. M. Mirzajanzadeh, T.N. Chakherlou, J. Vogwell, The effect of interference-fit on fretting fatigue crack initiation and DK of a single pinned plate in 7075 Al alloy, Engineering Fracture Mechanics. 78 (2011) 1233–1246.

[5]. B. Abazadeh, T.N. Chakherlou, R.C. Alderliesten, Effect of interference fitting and/or bolt clamping on the fatigue behavior of Al alloy 2024-T3 double shear lap joints in different cyclic load ranges, International Journal of Mechanical Sciences. 72 (2013) 2–12.

[6]. Chakherlou T, Mirzajanzadeh M, Abazadeh B, at al. An investigation about interference fit effect on improving fatigue life of a holed single plate in joints[J]. European Journal of Mechanics A/Solids, 2010,29:675-682.

[7]. B.G. Kiral, Effect of the clearance and interference-fit on failure of the pin-loaded composites, Materials and Design. 31 (2010) 85–93.

[8]. Zeng C, Tian W, Liao WH. The effect of residual stress due to interference fit on the fatigue behavior of a fastener hole with edge cracks[J]. Engineering Failure Analysis, 2016,66:72-87.

[9]. J.H. Deng, C. Tang, M.W. Fu, Y.R. Zhan, Effect of discharge voltage on the deformation of Ti Grade 1 rivet in electromagnetic riveting, Materials Science and Engineering: A. 591 (2014) 26-32.

[10]. U.A. Khashaba, T.A. Sebaey, A.I. Selmy, Experimental verification of a progressive damage model for composite pinned-joints with different clearances, International Journal of Mechanical Sciences. 152 (2019)481–491.

[11]. C. Chen, D. Hua, Q.M. Liu, X. Han, Evaluation on the interval values of tolerance fit for the composite bolted joint, Composite Structures. 206 (2018) 628–636.

[12]. P. Zou, Y. Li, K. Zhang, P. Liu, H. Zhong, Mode I delamination mechanism analysis on CFRP interference-fit during the installation process, Materials & Design. 116 (2017) 268-277.

[13]. Wang Z, Chang Z, Luo Q, et al. Optimization of riveting parameters using Kriging and particle swarm optimization to improve deformation homogeneity in aircraft assembly[J]. Advances in Mechanical Engineering, 2017,9(8):1-13.

[14]. J.J. Cui, L. Qi, H. Jiang, G.Y. Li, X. Zhang, Numerical and experimental investigations in electromagnetic riveting with different rivet dies, International Journal of Material Forming. 11 (2018) 839–853.

[15]. H. Jiang, Y. Cong, J. Zhang, X. Wu, G. Li, J. Cui, Fatigue response of electromagnetic riveted joints with different rivet dies subjected to pull-out loading, International Journal of Fatigue. 129 (2019) 1–13.

[16]. Y. Ma, M. Lou, Y. Li, Z. Lin, Effect of rivet and die on self-piercing rivetability of AA6061-T6 and mild steel CR4 of different gauges, Journal of Materials Processing Technology. 251 (2018) 282-294.

[17]. X. Wang, Z. Qi, K. Chen, Y. Liu, E. Wang, Study on the forming accuracy of the three-cylinder crankshaft using a specific die with a preformed dressing, The International Journal of Advanced Manufacturing Technology. 104 (2019) 551-564.

[18]. Y.X. Liu, B. Tang, L. Hua, H.J. Mao, Investigation of a novel modified die design for fine-blanking process to reduce the die-roll size, Journal of Materials Processing Tech. 260 (2018) 30–37.

[19]. Y. Lu, K. Ripplinger, X.J. Huang, Y. Mao, D. Detwiler, A.A. Luo A new fatigue life model for thermally-induced cracking in H13 steel dies for die casting, Journal of Materials Processing Tech. 271 (2019) 444–454.

[20]. Z. Qi, X. Wang, W. Chen, A new forming method of straight bevel gear using a specific die with a flash, The International Journal of Advanced Manufacturing Technology. 100 (2018) 3167-3183.

[21]. G.P. Syrcos, Die casting process optimization using Taguchi methods, Journal of materials processing technology. 135 (2004)68–74.

[22]. X. Zhang, M. Zhang, L. Sun, C. Li, Numerical simulation and experimental investigations on TA1 titanium alloy rivet in electromagnetic riveting, Archives of Civil and Mechanical Engineering. 18 (2018) 887-901.

[23]. J. Mucha, The numerical analysis of the effect of the joining process parameters on self-piercing riveting using the solid rivet, Archives of Civil and Mechanical Engineering. 14 (2014) 444-454.

[24]. Y. Zuo, Z. Cao, Y. Cao, Q. Zhang, W. Wang, Dynamic behavior of CFRP/Ti single-lap pinned joints under longitudinal electromagnetic dynamic loading, Composite Structures. 184 (2018) 362-371.

[25]. J. Hu, K. Zhang, Q. Yang, H. Cheng, P. Liu, Y. Yang, An experimental study on mechanical response of single-lap bolted CFRP composite interference-fit joints, Composite Structures. 196 (2018) 76-88.